Research Article

Yatong An, Ziping Liu and Song Zhang*

Evaluation of pixel-wise geometric constraint-based phase-unwrapping method for low signal-to-noise-ratio (SNR) phase

DOI 10.1515/aot-2016-0048
Received August 31, 2016; accepted November 8, 2016; previously published online December 15, 2016

Abstract: This paper evaluates the robustness of our recently proposed geometric constraint-based phase-unwrapping method to unwrap a low-signal-to-noise ratio (SNR) phase. Instead of capturing additional images for absolute phase unwrapping, the new phase-unwrapping algorithm uses geometric constraints of the digital fringe projection (DFP) system to create a virtual reference phase map to unwrap the phase pixel by pixel. Both simulation and experimental results demonstrate that this new phase-unwrapping method can even successfully unwrap low-SNR phase maps that bring difficulties for conventional multi-frequency phase-unwrapping methods.

Keywords: 3D shape measurement; noise; phase retrieval; phase unwrapping.

1 Introduction

Robustly unwrapping highly noisy, or low-signal-to-noise ratio (SNR), phase map is always a challenge for any phase-measurement profilometry. For both spatial and temporal phase-unwrapping algorithms, the most significant problem caused by noise is incorrect fringe order determination. One of the fundamental problems associated with conventional spatial or temporal phase-unwrapping algorithm lies in the fact that the fringe order is determined by referring to noisy information either obtained from points around the point of interest (e.g. spatial phase unwrapping [1]) or from other information on the same point (e.g. temporal phase unwrapping [2–7]).

One approach to alleviate noise impact for fringe order determination is to reduce reference noise, which is done conventionally by filtering. However, if noise is large, filtering by itself induces problems. An et al. [8] recently developed a completely new phase-unwrapping method that attempted to use noise-free reference for fringe order determination. Instead of using a conventional spatial or temporal phase-unwrapping method, the proposed phase-unwrapping technique uses geometric constraints of the calibrated structured light system to create a virtual reference phase map at a virtual plane z_{min}. This phase map is called Φ_{min}, which is used to determine fringe order pixel by pixel and then unwrap the entire phase. As the reference phase map is artificially created and noise free, fringe order determination is only influenced by the noise of the phase point itself, making it potentially more robust than a typical conventional spatial or temporal phase-unwrapping method.

This paper evaluates the robustness of the geometric constraint-based phase-unwrapping method in comparison with one of the most popular temporal phase-unwrapping method: multi-frequency phase shifting algorithms [2–5]. Both simulation and experimental data find that the proposed method can successfully unwrap the low-quality phase that fails the typical multi-frequency phase-unwrapping methods unless a lot of frequencies are used. It is important to know that this geometric constraint-based phase-unwrapping method is not trouble free, as mentioned by An et al. [8]; it has two major limitations: 1) confined depth sensing range and 2) requirement of accurate z_{min} estimation for large depth range measurement. All evaluations and comparisons provided in this paper do not go beyond these limitations.

Section 2 explains the principle of the geometric constraint-based phase-unwrapping algorithm including the phase-shifting algorithm itself. Section 3 shows some simulation data to compare the conventional multi-frequency phase-shifting algorithm and the geometric

***Corresponding author: Song Zhang,** School of Mechanical Engineering, Purdue University, West Lafayette, IN 47906, USA, e-mail: szhang15@purdue.edu
Yatong An and Ziping Liu: School of Mechanical Engineering, Purdue University, West Lafayette, IN 47906, USA

constraint-based phase-unwrapping algorithm. Section 4 presents some experimental validations, and finally, Section 5 summarizes this paper.

2 Principle

2.1 Three-step phase-shifting algorithm

Phase-shifting algorithms are extensively used in optical metrology due to their numerous advantageous features including pixel-by-pixel phase retrieval, robustness to noise, and ambient light [9]. In this research, we use a single three-step phase-shifting algorithm to evaluate the robustness of the phase-unwrapping algorithm because a three-step phase-shifting algorithm uses the least required number of patterns to recover a phase that is typically noisy. The three-step phase-shifting algorithm with equal phase shifts can be mathematically described as

$$I_1(x, y) = I'(x, y) + I''(x, y)\cos(\phi - 2\pi/3), \tag{1}$$

$$I_2(x, y) = I'(x, y) + I''(x, y)\cos(\phi), \tag{2}$$

$$I_3(x, y) = I'(x, y) + I''(x, y)\cos(\phi + 2\pi/3), \tag{3}$$

where $I'(x, y)$ is the average intensity, $I''(x, y)$ is the intensity modulation, and ϕ is the phase to be solved for. Solving Eqs. (1)–(3) simultaneously leads to

$$\phi(x, y) = \tan^{-1}\left[\frac{\sqrt{3}(I_1 - I_3)}{2I_2 - I_1 - I_3}\right]. \tag{4}$$

The phase obtained from Eq. (4) ranges from $-\pi$ to π with 2π discontinuities. A spatial or temporal phase-unwrapping algorithm is necessary to remove 2π discontinuities and obtain a continuous phase map by finding the proper integer number $k(x, y)$ of 2π for each pixel. The unwrapped phase is thus,

$$\Phi(x, y) = \phi(x, y) + k(x, y) \times 2\pi. \tag{5}$$

Here, $k(x, y)$ is also often referred to as fringe order. Conventional phase-unwrapping methods can be classified as spatial or temporal phase unwrapping: the former detects 2π discontinuous points by evaluating the phase values of neighboring pixels, and the latter captures additional images and detects 2π discontinuities by referring to additional captured information. As spatial phase unwrapping has limited capacities (e.g. single smooth geometry), the next section will discuss one of the most popular temporal phase-unwrapping methods: multi-frequency phase-unwrapping algorithm.

2.2 Multi-frequency phase unwrapping

A conventional temporal phase-unwrapping method determines fringe order $k(x, y)$ by referring to additional images captured by the camera (e.g. binary-coded patterns, fringe patterns with different frequencies). This paper only compares the proposed method with multi-frequency phase-unwrapping algorithms due to their robustness and extensive adoption. In brief, multi-frequency phase unwrapping works as follows: 1) capture a set of wrapped phase $\phi_k(x, y)$ (k = 2, 3, …) with different frequencies; 2) create an equivalent lowest-frequency phase map ϕ_{eq} by combining these high-frequency phase maps together, and ϕ_{eq} does not have any 2π discontinues (or regarded as unwrapped phase $\Phi_{eq} = \phi_{eq}$; and 3) unwrap higher-frequency phase maps by referring to the lower-frequency unwrapped phase maps. For example, for a two-frequency phase-shifting algorithm [2], assuming the fringe periods are T_1 and T_2, with $T_1 > T_2$, the equivalent fringe period is

$$T_{eq} = \frac{T_1 T_2}{T_1 - T_2}, \tag{6}$$

and the equivalent phase map is

$$\Phi_{eq} = \phi_{eq} = \phi_2 - \phi_1 \mod 2\pi. \tag{7}$$

Here mod is the modulus operator. Backward phase unwrapping can be performed sequentially by determining the corresponding fringe orders:

$$k_1(x, y) = \text{Round}\left[\frac{\Phi_{eq}\frac{T_{eq}}{T_1} - \phi_1}{2\pi}\right], \tag{8}$$

$$k_2(x, y) = \text{Round}\left[\frac{\Phi_1\frac{T_1}{T_2} - \phi_2}{2\pi}\right]. \tag{9}$$

Here, Round(x) is to take the closest integer number of variable x.

$$\Phi_1 = \phi_1 + k_1(x, y) \times 2\pi, \tag{10}$$

$$\Phi_2 = \phi_2 + k_2(x, y) \times 2\pi, \tag{11}$$

denote the unwrapped phase maps. Similarly, if more frequencies, shorter and shorter-frequency phase maps can be unwrapped by the longer ones sequentially.

Despite their extensive employment, the multi-frequency phase-shifting algorithms have one common

problem: the inherent noise of additional images (i.e. phase maps) could lead to incorrect fringe order. For example, Eq. (8) indicates that if $\frac{T_{eq}}{T_1}=20$, the 0.16 rad phase noise in Φ_{eq} could lead to a wrong fringe order k_1. Therefore, to reduce noise impact, one usually has to reduce scaling factor $\frac{T_{eq}}{T_1}$ for any given system settings. However, reducing the scaling factor often means capturing fringe patterns of more frequencies. In contrast, if the reference phase Φ_{eq} is noise free, an arbitrary number of scaling factor can be used. In the next section, we will discuss such a phase-unwrapping method proposed recently by An et al. [8]. This new phase-unwrapping method refers to a noise-free phase map, and thus, we believe that this phase-unwrapping method can be used to unwrap the noisy phase that fails a typical temporal phase-unwrapping method.

2.3 Geometric constraint-based phase unwrapping

The newly proposed phase-unwrapping method unwraps a phase pixel by pixel by referring to a virtually created minimum phase map based on the geometric constraints of a structured light system. In brief, after the structured light system calibration, one can determine the geometric relationship between a 3D point in the world coordinate system and its projection to the camera and the projector 2D image coordinate system. Therefore, for a given virtual plane at z_{min}, the camera-sensed area can be mapped to the projector's area pixel by pixel. Figure 1A illustrates that for a given virtual plane at z_{min}, the camera-sensed area can be mapped to the projector's area pixel by pixel. The corresponding mapped projector area uniquely defines the phase map called the minimum phase Φ_{min}. If the real object is placed at a distance z, which is farther away from the camera, the mapped region on the projector changes accordingly, as illustrated in Figure 1B.

An et al. [8] demonstrated that if z is not too far away from z_{min}, the wrapped phase of the object being measured can be unwrapped pixel by pixel by referring to Φ_{min}. The maximum depth range that the method can handle without problems is

$$\Delta z=\frac{T_s}{\sin\alpha}, \tag{12}$$

where T_s is the single fringe pattern span on the object space; α is the angle between the projection direction and the capture direction; and Δz is the difference between the object depth z and z_{min} plane.

Figure 2 graphically illustrates the concept. Figure 2A shows the wrapped phase of the projection image, and the red and blue windowed region shows the camera-captured area at different depths. Figure 2B shows the defined continuous phase map on the projector. For the wrapped phase at a virtual plane z_{min}, the wrapped phase ϕ_1 can be unwrapped to create the Φ_{min} map. However, for an object positioned at an unknown distance z, only the wrapped phase ϕ can be obtained. Figure 2C illustrates the cross sections of the phase map. For the case with a single 2π jump, this figure shows that if ϕ is less than Φ_{min}, 2π should be added accordingly to unwrap ϕ. Figure 2D shows a case with two 2π discontinuous locations, 2π should be added to points if phase difference $\Delta\phi=\Phi_{min}-\phi$ is between 0 and 2π, and $2\times2\pi$ should be added if $2\pi<\Delta\phi<4\pi$.

In general, one can prove that fringe order $k(x, y)$ can be determined by

$$k(x, y)=ceil\left[\frac{\Phi_{min}(x, y)-\phi(x, y)}{2\pi}\right], \tag{13}$$

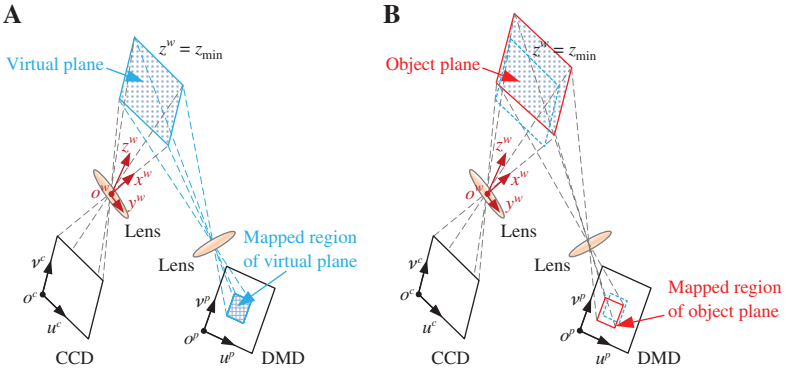

Figure 1: Graphical representation of mapped camera-sensing regions when an object is placed at different distances. (A) Mapped projection region for a virtual minimum plane $z=z_{min}$; (B) mapped projection region for an object at z.

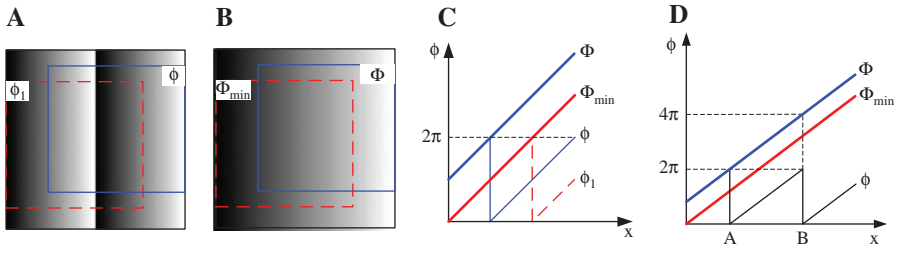

Figure 2: Conceptual idea of unwrapping phase using the minimum phase map determined from geometric constraints [8]. (A) Windowed regions show a phase map that was acquired by a camera when an object is at different depths: red dashed window shows at z_{min} and solid blue window shows at z; (B) Corresponding Φ_{min} and Φ on the projector; (C) Cross sections of Φ_{min} and Φ and the phase maps with one 2π discontinuous location; (D) Case with two 2π discontinuous locations.

where ceil[] is the ceiling operator that returns the closest upper integer value. Unlike Eq. (8) where fringe order is affected by noise from Φ_{eq}, fringe order $k(x, y)$ in Eq. (13) is affected solely by the inherent noise from $\phi(x, y)$ itself. In summary, the recently proposed phase-unwrapping method does not require additional image acquisition, yet still detects 2π discontinuities by referring to information inherent to structured light system constraints. Unlike conventional phase-unwrapping methods that require referring inherent noisy information for fringe order determination, this proposed method determines fringe order by referring to noise free information. Therefore, we believe that this new phase-unwrapping method can be used to unwrap the noisy phase that fails a typical conventional phase-unwrapping method (e.g. a multi-frequency phase-shifting method). The following two sections are to evaluate performance of this phase-unwrapping method against that of the multi-frequency temporal phase-unwrapping method.

3 Simulation

We simulated situations with different amounts of noise levels (or SNRs). Figure 3 shows examples of a system with SNRs of 40, 20, 10, and 5 (all are with a unit dB, the same in the following). The first row of this figure shows one of three phase-shifted fringe patterns, and the second row shows the corresponding wrapped phase maps. Note that to better visualize the images, only a small section of the images are shown here.

Equation (12) provides the maximum depth range Δz that the geometric constraint-based phase-unwrapping method can handle. Yet, for noisy conditions, the effective range is reduced. In all these simulations, we assume that the object depth range is 50% of Δz, and the z_{min} is approximately 25% of Δz away from the object's nearest point to the camera. We then apply Φ_{min} to unwrap all four levels of noisy phase maps, from which 3D geometries are recovered. The first row images of Figure 4 show 3D results.

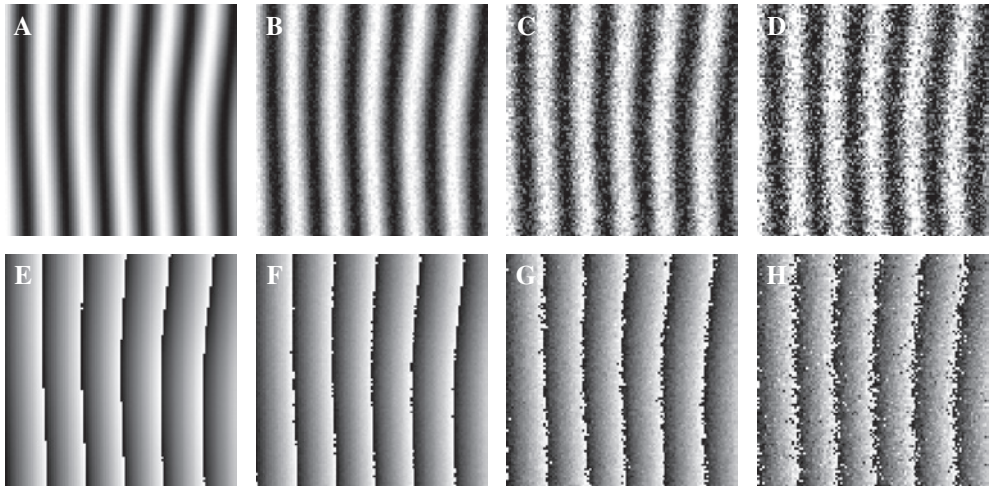

Figure 3: Fringe patterns and associated phase at different SNR values. (A)–(D) One of three phase-shifted fringe patterns; (E)–(H) wrapped phase map. (A and E) SNR = 40, (B and F) SNR = 20, (C and G) SNR = 10, (D and H) SNR = 5.

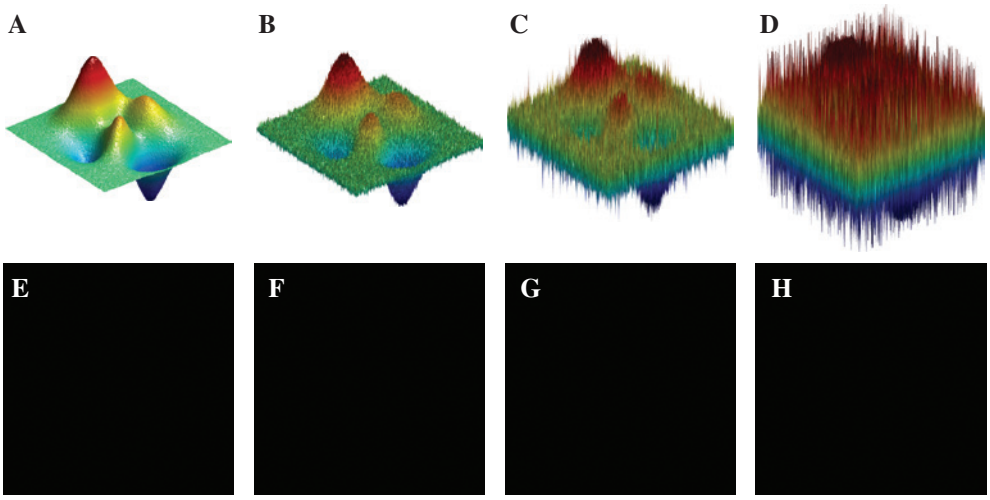

Figure 4: Phase reconstructions using Φ_{min} under different SNR values. (A)–(D) 3D reconstruction; (E)–(H) zoom-in view of incorrectly unwrapped points (white dots). (A and E) SNR = 40, (B and F) SNR = 20, (C and G) SNR = 10, (D and H) SNR = 5.

To quantify the unwrapping effectiveness, we identify total incorrectly unwrapped-phase points by

$$E(i,j)=\begin{cases} true & |\Phi^n-\Phi^i|>1.5\pi \\ false & otherwise \end{cases}, \tag{14}$$

where Φ^n is the recovered phase point with noise, and Φ^i is the ideal phase without noise. The condition of 1.5π is chosen because if a point is not correctly unwrapped, the difference should be an integer number of 2π.

The second row images of Figure 4 show the incorrectly unwrapped points (marked as white). Clearly all points are correctly unwrapped (the entire images are all black) even when the SNR is as low as 5.

We then employ the three-frequency phase-unwrapping method to unwrap those phase maps shown in Figure 3. The high-frequency fringe period is 24 pixels, the low-frequency fringe period is 720 pixels, and the median-frequency fringe period is 132 pixels. Figure 5 shows the result. When fringe patterns are of high quality (SNR = 40 or 20), a three-frequency phase-shifting algorithm can properly unwrap the entire phase. However, when the noise level reduces to SNR = 10 or 5, many points are incorrectly unwrapped such that the original

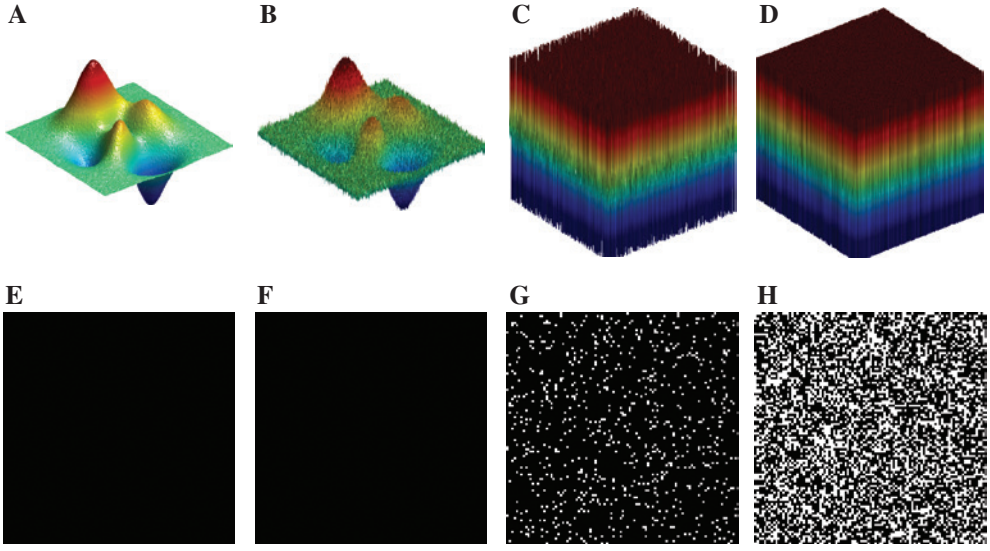

Figure 5: Phase reconstructions using three-frequency phase-shifting algorithm under different SNR values. (A)–(D) 3D reconstruction; (E)–(H) zoom-in view of incorrectly unwrapped points (white dots). (A and E) SNR = 40, (B and F) SNR = 20, (C and G) SNR = 10, (D and H) SNR = 5.

3D geometry cannot be apparent as shown in Figures 5C and D.

One approach to reduce the incorrectly unwrapped points is to increase the number of frequencies for the multi-frequency phase-shifting algorithm. For SNR = 10, we simulate such a case by increasing the number of frequencies up to 10, and Figure 6 shows the results of four- to seven-frequency phase-shifting algorithms. These results indicate that with the number of frequencies increasing, the number of incorrectly unwrapped phase points decreases (until 0), as expected, as the noise impact from reference phase maps decreases due to the use of smaller scaling factors.

To quantify the influence of using different numbers of frequencies, we identify the incorrectly unwrapped points for different noise levels and for 2- to 10-frequency phase-shifting algorithms and compute the percentage of incorrectly unwrapped points over the overall pixel number. Figure 7 shows the result. Figure 7D indicates that even if one applies the 10-frequency phase-shifting algorithm, approximately 6% of the points are still not correctly unwrapped.

It is important to notice that filtering can improve the multi-frequency phase unwrapping, but none of the simulation uses any filters to fairly compare these two methods. The multi-frequency phase-unwrapping algorithm can handle arbitrary depth-range sensing, but all simulations are carried out for a depth range of approximately 50% of Δz from Eq. (12). These results clearly demonstrate that, for a limited depth-range sensing, the geometric constraint-based phase-unwrapping method can unwrap the highly noisy phase that fails the conventional multi-frequency phase-unwrapping algorithms if the number of frequency is not extremely large.

4 Experiments

We also carried out experiments to further evaluate the performance of our phase-unwrapping algorithm

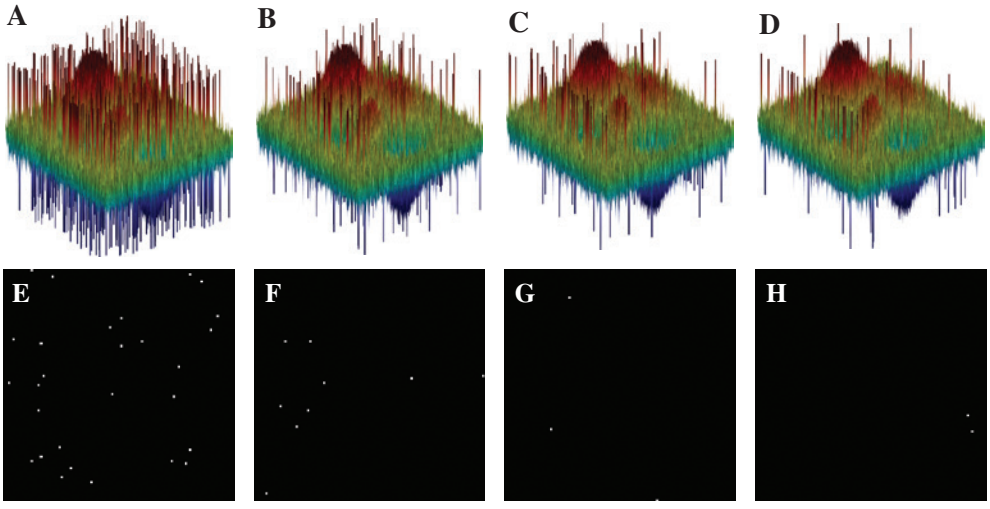

Figure 6: Phase reconstructions using different numbers of frequency phase-shifting algorithm under the same SNR value (SNR = 10). (A)–(D) 3D reconstruction; (E)–(H) zoom-in view of incorrectly unwrapped points (white dots). (A and E) F = 4, (B and F) F = 5, (C and G) F = 6, (D and H) F = 7.

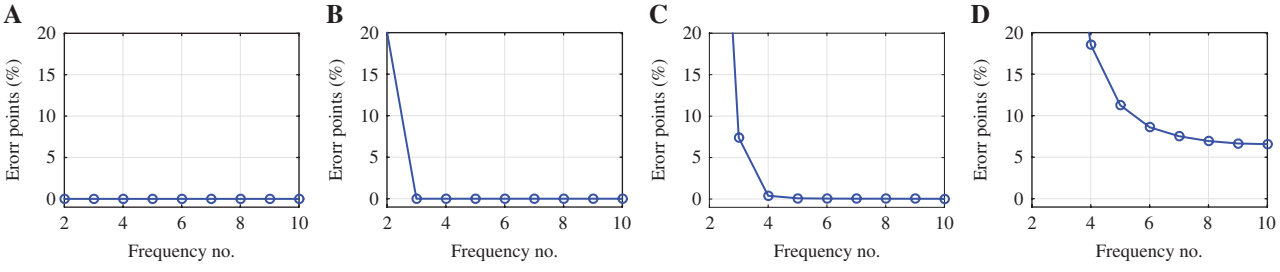

Figure 7: Incorrectly unwrapped point percentage for different frequency numbers and different SNR values. (A) SNR = 40, (B) SNR = 20, (C) SNR = 10, (D) SNR = 5.

under noisy conditions. The hardware system consists of one single CCD camera (Model: The Imaging Source DMK23U618, The Imaging Source, Charlotte, NC, USA) and one digital light processing (DLP) projector (Model: Dell M115HD, Dell Inc., Round Rock, TX, USA). The camera resolution is 640×480, and it is attached with an 8-mm focal length lens (Model: Computar M0814-MP2, CBC AMERICAS Corp., Cary, NC, USA). The projector's native resolution is 1280×800 with a 14.95-mm fixed focal length lens. The entire system was calibrated using the calibration approach developed by Li et al. [10]. It should be noted that during the entire experiments, the whole system settings, including exposure time and aperture of the camera, remained the same.

Figure 8A shows one photograph of a puppy toy that has black hair and yellow legs. Apparently, this type of object is very difficult to measure especially using a three-step phase-shifting algorithm due to complex structure and low contrast. Figure 8B shows one of three phase-shifted fringe patterns, demonstrating that the fringe contrast is very low (i.e. low SNR). Applying the three-step phase-shifting algorithm yielded the wrapped phase map shown in Figure 8C. Again, a large noise is apparent on the phase map. We then applied a three-frequency phase-unwrapping method with three fringe periods of 36, 162, and 800 pixels to temporally unwrap the phase map. Figure 8D shows a 3D reconstruction using the temporally unwrapped phase map: numerous points are not properly measured (holes on the geometry). We then applied the geometric constraint-based phase-unwrapping method to unwrap the wrapped phase map shown in Figure 8C, and Figure 8E shows the corresponding 3D reconstruction. This experiment indicates that our proposed method can successfully reconstruct the entire geometry without apparent spiky noise. As a comparison, we also measured the same object with more-step phase-shifting algorithm to obtain the Ground Truth. Figure 8F shows the result. In this experiment, we used a 10-frequency phase-shifting algorithm for temporal phase unwrapping and captured 18 equally phase-shifted fringe patterns for each frequency to reduce noise impact.

To better visualize the difference, close-up views are generated. Figure 9A and B, respectively, shows the close-up 3D reconstruction result of Figure 8D and E. Figure 9C shows the close-up view of the ground truth geometry. As one can see, the result obtained from the geometric-constraints based method is almost identical to the ground truth, suggesting the robustness of the geometric constraint-based phase-unwrapping method.

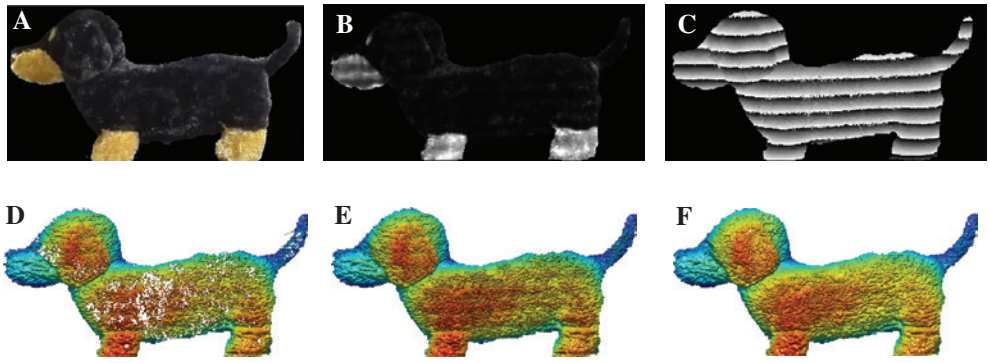

Figure 8: Phase-unwrapping comparison between the conventional method and our proposed method. (A) Photography of the testing object. (B) One of the three phase-shifted fringe images. (C) Wrapped phase. (D) 3D geometry reconstructed from the phase obtained by a three-frequency phase-shifting method. (E) 3D geometry reconstructed by the phase obtained from geometric constraint-based phase-unwrapping method. (F) Ground truth 3D geometry.

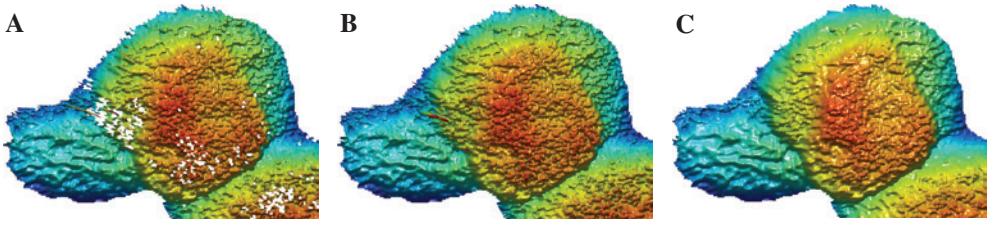

Figure 9: Close-up views of 3D results. (A) Close-up view of 3D geometry shown in Figure 8D. (B) Close-up view of 3D geometry shown in Figure 8E. (C) Close-up view of 3D geometry shown in Figure 8F.

Similar to simulations, we further evaluated the performance of the different-frequency phase-shifting algorithms by measuring the same object. Figure 10 shows the results. In all these experiments, only the three-step phase-shifting algorithm is used for each frequency pattern. As one can see, with the increasing number of frequencies, more and more data points are properly measured, as expected. Figure 10F shows the 3D result from the nine-frequency phase-shifting algorithm, which is comparable to the result show in Figure 9B, although there are still a few spikes in the entire measurement. These experiments demonstrate that one can, indeed, use the three-step phase-shifting algorithm for each frequency but use a lot of frequencies to perform reasonable quality measurement.

As our proposed phase-unwrapping algorithm can obtain an absolute phase, it is possible to measure multiple isolated objects simultaneously. Figure 11 shows a measurement example. Figure 11A is the photograph of the two isolated objects. Again, we used three phase-shifted fringe patterns and compute the wrapped phase. Figure 11B shows one fringe pattern, and Figure 11C is the wrapped phase. Figure 11D shows the result from the conventional two-frequency method. Clearly, the two-frequency phase-unwrapping algorithm does not work well because there are many holes on the recovered 3D geometry. Figure 11E shows the result from the seven-frequency phase-shifting algorithm; almost the entire 3D geometry is correctly reconstructed. We then used our proposed phase-unwrapping algorithm to unwrap the same phase shown in Figure 11C; the entire geometry can be properly recovered, as shown in Figure 11F. This experiment demonstrated that our proposed phase-unwrapping algorithm is, indeed, similar to a temporal phase-unwrapping

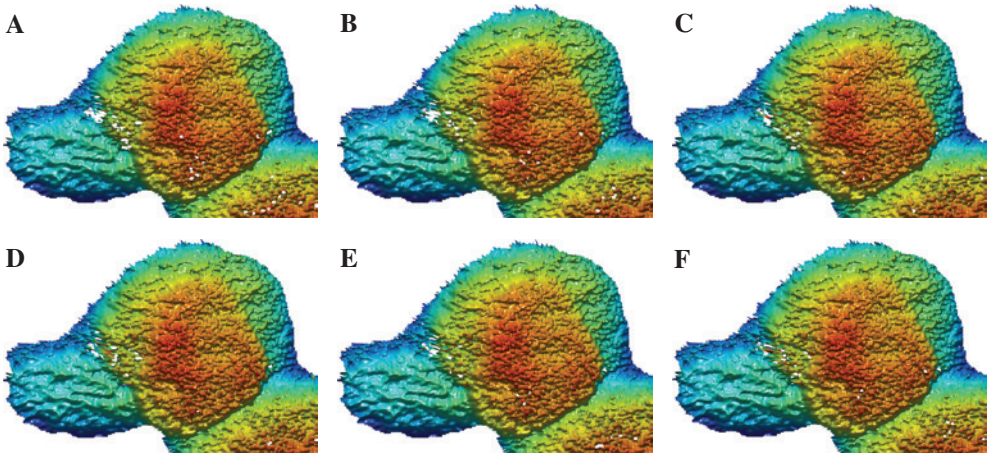

Figure 10: Experimental data with increasing number for frequencies used. (A)–(F) The numbers of frequencies used are 4, 5, 6, 7, 8, 9, respectively.

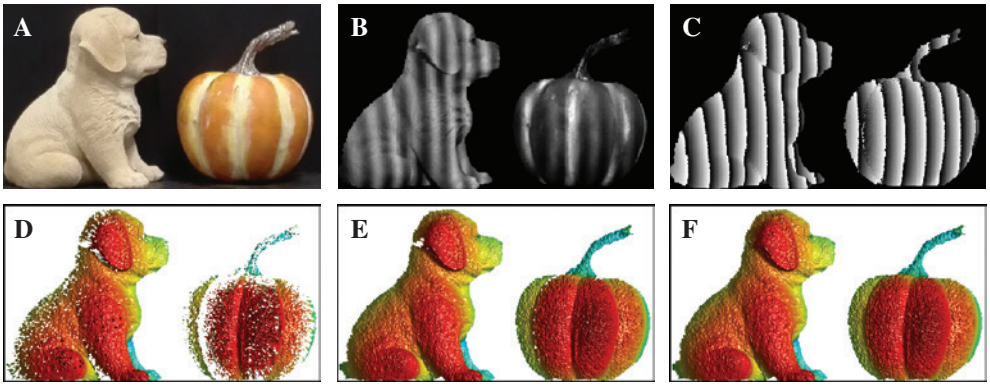

Figure 11: Measurement results of two isolated objects. (A) Photograph of the objects. (B) One of the three phase-shifted fringe images. (C) Wrapped phase. (D) 3D geometry reconstructed from the unwrapped phase obtained by a two-frequency phase-unwrapping method. (E) 3D geometry reconstructed from the unwrapped phase obtained by a seven-frequency phase-unwrapping method. (F) 3D geometry reconstructed by the unwrapped phase obtained by our proposed geometric constraint-based phase-unwrapping method.

algorithm and can be used to measure isolated objects properly. This is fundamentally different from a spatial phase-unwrapping algorithm as a spatial phase-unwrapping algorithm typically cannot be used to measure the absolute geometries of multiple isolated objects.

Despite its robustness to unwrap the noisy phase map, this novel phase-unwrapping method has the following two major limitations: 1) confined depth range and 2) requirement of accurate $z_{\min}$ estimation. Equation (12) indicates that one can reduce the angle between the projector and the camera or increase the fringe period to enlarge the depth-sensing range. However, changing those parameters is not desirable as it compromises the measurement quality. Therefore, for large depth-range sensing, this method, itself, still cannot work, and it requires a combination with other temporal phase-unwrapping methods.

5 Summary

This paper has evaluated the performance of our recently developed geometric constraint-based phase-unwrapping algorithm. Through simulation and experiments, we have demonstrated that this new phase-unwrapping approach outperforms the conventional multi-frequency phase-unwrapping algorithms when phase is noisy and the number of frequencies is not large. However, due to the use of the virtual plane for minimum phase creation, this newly developed phase-unwrapping method has its confined depth-sensing range and requires accurate estimation of $z_{\min}$ to maximize the depth-sensing range.

Acknowledgment: This study was sponsored by the National Science Foundation (NSF) under grant numbers CMMI-1521048. The views expressed in this paper are those of the authors and not necessarily those of the NSF.

References

[1] D. C. Ghiglia and M. D. Pritt, eds., 'Two-Dimensional Phase Unwrapping: Theory, Algorithms, and Software', (John Wiley and Sons, New York, 1998).
[2] Y.-Y. Cheng and J. C. Wyant, Appl. Opt. 23, 4539–4543 (1984).
[3] Y.-Y. Cheng and J. C. Wyant, Appl. Opt. 24, 804–807 (1985).
[4] D. P. Towers, J. D. C. Jones and C. E. Towers, Opt. Lett. 28, 1–3 (2003).
[5] Y. Wang and S. Zhang, Opt. Express 19, 5143–5148 (2011).
[6] G. Sansoni, M. Carocci and R. Rodella, Appl. Opt. 38, 6565–6573 (1999).
[7] S. Zhang, Opt. Lett. 35, 931–933 (2010).
[8] Y. An, J.-S. Hyun and S. Zhang, Opt. Express 24, 18445–18459 (2016).
[9] D. Malacara, ed., 'Optical Shop Testing', 3rd ed (John Wiley and Sons, New York, NY, 2007).
[10] B. Li, N. Karpinsky and S. Zhang, Appl. Opt. 53, 3415–3426 (2014).

Yatong An
School of Mechanical Engineering, Purdue University, West Lafayette, IN 47906, USA

Yatong An is currently a PhD student in the School of Mechanical Engineering at Purdue University. He received his MPhil degree in Computer Science from the University of Hong Kong in August 2015. In 2013, he received his BS degree from the Department of Control Science and Engineering in Zhejiang University, China. His research interests include optical measurement, 3D reconstruction, computer vision, control, robotics, and machine learning.

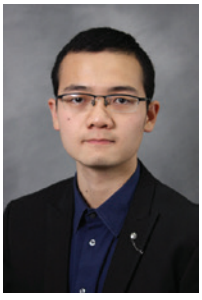

Ziping Liu
School of Mechanical Engineering, Purdue University, West Lafayette, IN 47906, USA

Ziping Liu is an undergraduate student in the School of Mechanical Engineering at Purdue University. He is currently working with Dr. Zhang as an undergraduate research assistant in the XYZT Lab. His research interests include high-speed 3D optical metrology and computational imaging.

Song Zhang
School of Mechanical Engineering, Purdue University, West Lafayette, IN 47906, USA
szhang15@purdue.edu

Song Zhang is an associate professor of Mechanical Engineering at Purdue University. He received his PhD degree in Mechanical Engineering from Stony Brook University in 2005. He was a postdoctoral fellow at Harvard University for 3 years and joined Iowa State University as an assistant in 2008 before moving to Purdue in 2015. He won the AIAA Best Paper Award, Best of SIGGRAPH by the Walt

Disney, NSF CAREER award, Stony Brook University's "40 under 40 Alumni Award", and Discovery in Mechanical Engineering Award. He is a fellow of SPIE-the International Society for Optics and Photonics, and a senior member of Optical Society of America (OSA). His current research focuses on developing superfast, super-resolution 3-D imaging technologies and on exploring their applications.